Dual-current-injection CSCC Active Common-mode EMI Filters with High Insertion Loss for DC-DC Converters*

Hong Li[1*], *Siyi Wang*[1], *Chongmo Zhang*[1] *and Bo Zhang*[2]

(1. School of Electrical Engineering, Beijing Jiaotong University, Beijing 100044, China;
2. School of Electric Power Engineering, South China University of Technology, Guangzhou 510641, China)

Abstract: With the increase in the switching frequency and power density, DC-DC converters encounter more severe electromagnetic interference (EMI) problems. To suppress the common-mode EMI generated by converters, as well as maintain the high-power-density of converters, the active EMI filter (AEF) has attracted increasing interest owing to its small volume. The EMI suppression effect of the common single-stage single-sense single-injection AEF is confined because of the limited insertion loss, and the volume of the multi-stage AEF will be bulky. To solve this problem, this paper proposes a compact dual-current-injection current-sense current-compensation (DCJ-CSCC) AEF to increase the insertion loss in the entire conducted EMI frequency band, as well as considering the volume of the AEF. The structure and operating principle of the proposed AEF are introduced. Finally, taking a boost converter as an example, the effectiveness and advantages of the proposed DCJ-CSCC AEF were verified through a simulation and experiment, the results show that the proposed AEF has a better EMI suppression effect on the entire conducted EMI frequency band with a similar volume compared with existing single-injection feedforward current-sense current-compensation (FF-CSCC) and feedback current-sense current-compensation (FB-CSCC) AEFs. This paper provides a new selection for EMI suppression in DC-DC converters.

Keywords: Electromagnetic interference, active EMI filter, common-mode, electromagnetic compatibility

1 Introduction

The main source of electromagnetic interference (EMI) in power converters is primarily the rapid action of switching devices, which results in the rapid change of voltage and current, and it propagates through a conducted or radiated path to reach sensitive equipment [1-3]. Currently, as the higher power density and higher switching frequency of the converters are required to realize low cost and light weight, the EMI problem of power converters is becoming increasingly severe [4]. To solve the EMI problem, the common methods are added EMI filters in power converters [5]. EMI filters are classified into passive EMI filters (PEFs) and active EMI filters (AEFs) [6]. PEFs are more widely used in industrial equipment due to its low cost and simple circuits [7].

The conduction form of EMI can be divided into common-mode (CM) and differential-mode (DM) interference. CM PEFs composed of common-mode (CM) chokes and Y-capacitors are usually applied on the power input side of an equipment under test (EUT). Although the EMI filter can be easily implemented, it has some limitations. A large Y-capacitor may cause dangerous leakage currents exceeding safety regulation limits and is therefore prohibited. In addition, the CM inductor windings conduct full power currents so the CM inductors are usually large, which is unsuitable for the traditional CM PEFs to be applied in high power density power converters. Further, in high frequency power converters, the parasitic parameters of PEFs cause a negative impact on high frequency band for EMI suppression [8].

Manuscript received October 20, 2022; revised November 10, 2022; accepted November 21, 2022. Date of publication December 31, 2022; date of current version December 9, 2022.
* Corresponding Author, E-mail: hli@bjtu.edu.cn
* Supported in part by the Royal Academy of Engineering: Transforming Systems through Partnership (China) under Grant TSPC1017; in part by the Excellent Youth Scholars of National Natural Science Foundation of China under Grant 51822701, in part by the Key Project of National Natural Science Foundation of China and Smart Grid Joint Fund of State Grid Corporation of China under Grant U1866211.
Digital Object Identifier: 10.23919/CJEE.2022.000035

Therefore, compared with DM PEFs, CM PEFs is more difficult to satisfy the strict requirement of high power density on DC-DC converters.

The EMI suppression principle of AEFs is fundamentally different from that of PEFs: sense the noise signal and use the amplification part to generate a reverse signal for interference cancellation [9]. The AEFs have the advantages in high integration and small sizes, which make AEFs more suitable for the high power density DC-DC converters.

AEFs can be typically classified into analog and digital AEFs. Digital AEFs are designed and implemented using programmable chips [10-11], whose structure and design process are relatively complex and the costs are expensive. Analog AEFs are frequently designed using operational amplifiers (OPAMs), bipolar transistors, etc., whose structures are relatively simple and the costs are much cheaper than digital AEFs.

The existing single-sense single-injection AEFs can be one stage structure or multi-stage structure [12]. For the one stage AEF, its insertion loss is limited due to the limited amplification gain. Therefore, the single-sense single-injection AEFs usually cannot achieve satisfied EMI suppression effect in circuits that greatly exceed EMI standard.

To solve the problem of the limited filtering effect of single-sense single-injection AEFs, scholars have developed several configurations: AEFs and PEFs are combined to form hybrid EMI filters to improve the overall filtering effect [13-16]. However, such a hybrid EMI filter still contains a bulky inductor, which conflicts with the original intention of AEFs to reduce the volume. In Ref. [17], chaotic pulse-width modulation (PWM) for PWM converters was combined with AEFs to improve the high-frequency suppression effect of AEFs, however, this method is only applicable to PWM converters, therefore, the application scenarios of this method are limited. Additionally, a two-stage cascaded AEF was designed to improve the overall filtering effect of an AEF in Ref. [18], in which most of the two-stage cascade topologies of AEFs were analyzed, and the combination of voltage-sense current-compensation (VSCC) and current-sense current-compensation (CSCC) AEFs is proved to be the best combination for EMI filtering. However, the volume and the cost of the two-stage cascade AEF are almost as double as that of a single-stage one.

To use one stage AEF to achieve the EMI filtering effect of a two-stage AEF, this paper proposes a new dual-current-injection AEF topology (hereinafter called the DCJ-CSCC AEF) for CM noise suppression. The remainder of this paper is arranged as follows: in Section 2, the topology and ideal equivalent model of the proposed DCJ-CSCC AEF is presented; in Section 3, the operation principle of the DCJ-CSCC AEF is introduced, whose EMI filtering effect is quantitatively analyzed. Taking a boost converter as an example, the EMI filtering effect of the DCJ-CSCC AEF is verified and compared with that of the typical feedforward-CSCC (FF-CSCC) or feedback-CSCC (FB-CSCC) AEFs. In Section 4, the experiment results are given. Finally, the conclusions are drawn in Section 5.

2 Topology and equivalent model of the DCJ-CSCC AEF

The equivalent circuit of CM EMI of a DC-DC converter can be modeled as Fig. 1. The CM noise can be represented with an equivalent noise current source I_n in parallel with an equivalent impedance Z_n. The impedance of line impedance stabilization network (LISN) is often used to measure the intensity of CM noise, which is represented by Z_{LISN} in the measuring circuit. The noise current flowing through the load is I_L.

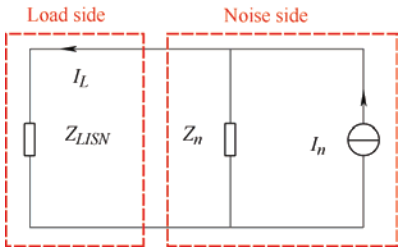

Fig. 1 CM EMI model of a DC-DC converter

Fig. 2 shows the AEF equivalent model and its installation position in converters. Basically, an AEF at least contains three parts: sensing part, amplification part, and injection part. The current transformer (CT) is used to sense current, then, the sensing signal is amplified by the amplification part, after the amplification, the AEF can generate a signal in reverse of the sensed noise signal, namely, Av_x. Finally, the

reverse injection currents I_{AEF} is injected into the main circuit by capacitor to suppress CM EMI.

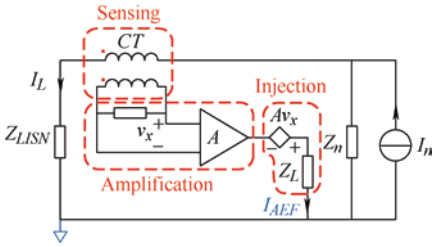

Fig. 2 Basic structure of AEF and its installation position

2.1 Equivalent model of the existing FF- CSCC AEF and FB-CSCC AEF

The existing popular topologies of AEFs are FB-CSCC AEF and FF-CSCC AEF [9-12], as shown in Fig. 3. Where, V_{out} is the signal in reverse of the sensed noise signal, R_{inj} and C_{inj} are the output impedances of the AEF, I_{AEF} is the injection current of the AEF. $A_1(s)$ or $A_2(s)$ represents the total gain of FB-CSCC AEF or FF-CSCC AEF.

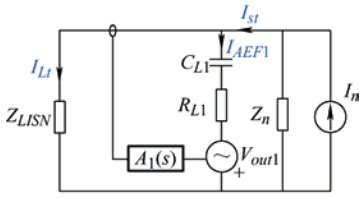

(a) FB-CSCC AEF

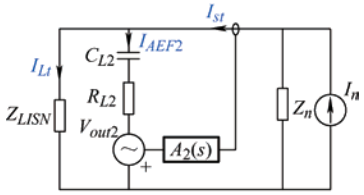

(b) FF-CSCC AEF

Fig. 3 The equivalent models of FF-CSCC and FB-CSCC AEF

Based on Fig. 3, the injection currents of FB-CSCC AEF or FF-CSCC AEF can be expressed by Eqs. (1) and (2), respectively.

$$I_{AEF1}(s)=\frac{I_{LI}Z_{LISN}(s)-V_{out1}}{Z_{inj1}(s)}=\frac{I_{LI}Z_{LISN}(s)-I_{LI}G_1(s)}{Z_{inj1}(s)} \tag{1}$$

$$I_{AEF2}(s)=\frac{I_{LI}Z_{LISN}(s)-V_{out2}}{Z_{inj2}(s)}=\frac{I_{LI}Z_{LISN}(s)-(I_{LI}+I_{AEF2})G_2(s)}{Z_{inj2}(s)} \tag{2}$$

In practical applications, DC-DC converters often need two-stage EMI filtering to meet the EMC standards [18], as seen in Fig. 4.

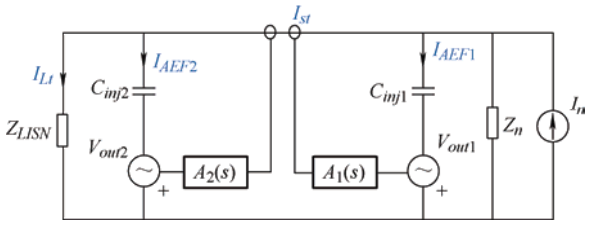

Fig. 4 Equivalent model of two-stage cascade CSCC AEF

But if a two-stage AEF is used, its volume and the devices number of the AEF will be almost double comparing with that of one-stage AEF, which will reduce the power density of DC-DC converters obviously.

2.2 Topology and ideal equivalent model of DCJ-CSCC AEF

To solve the problem above, namely, to make the one-stage AEF have the same CM EMI filtering ability with the two-stage AEF, this paper proposes a new AEF topology, namely, DCJ-CSCC AEF, based on the superposition principle, and its equivalent model is shown in Fig. 5.

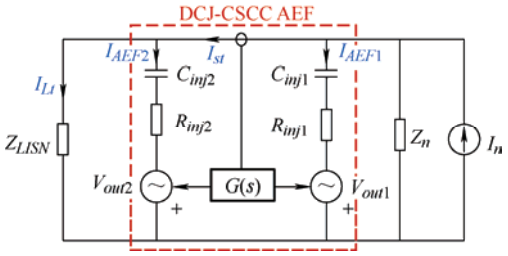

Fig. 5 Equivalent model of DCJ-CSCC AEF

The basic idea is to integrate the FB-CSCC AEF and FF-CSCC AEF in one CSCC AEF by using the dual injection way and using one feedback link to realize the feedback and feedforward at the same time. In Fig. 5, I_{AEF1} and I_{AEF2} are the FF injection current and FB injection current, respectively.

The detailed topology of the proposed DCJ-CSCC AEF is shown in Fig. 6, it is also composed of a sensing part, i.e. a current transformer (CT), an amplification part, i.e. a high-frequency OPAM circuit, and a push-pull amplifier circuit with bipolar junction transistors (BJTs), and an injection part, i.e. the injection capacitors.

Where, the current flowing through the LISN is I_{lisn}, R_{in} is used to convert the sensed CM current into

voltage. R_{bias} and D_1, D_2 in the push-pull amplifier circuit are used to adjust the quiescent point of the amplifier. R_L and C_L are the output loads of the push-pull amplifier. The output voltage of OPAM circuit is converted into injection current through R_L and C_L and coupled to the ground. The injection current generated by the push-pull amplifier flows into the power line by feedback injection capacitor C_{inj1} and feedforward injection capacitor C_{inj2}, respectively.

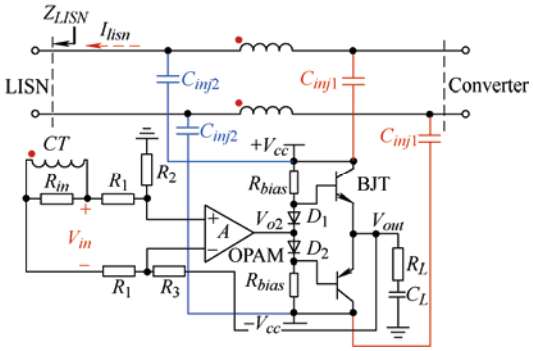

Fig. 6 Topology of the proposed DCJ-CSCC AEF

3 Operation principle of the DCJ-CSCC AEF

In order to describe the CM EMI filtering effect of the DCJ-CSCC AEF clearly, the insertion loss of AEF should be calculated firstly. A higher insertion loss indicates that after adding the filter, the amplitude of noise attenuation is larger, that is to say, the filter has a better filtering effect. As is known to all, the effective operating frequency band of an AEF in practical application is 150 kHz-30 MHz, thus, the ideal model shown in Fig. 5 is not accurate enough for calculating the insertion loss of an AEF and a high-frequency AEF model is necessary. In this section, the high-frequency models of CT, OPAM and BJTs in the proposed DCJ-CSCC AEF are given to obtain the insertion loss expression of the DCJ-CSCC AEF.

3.1 CT Modeling in DCJ-CSCC AEF

The CM signal sensing function of CT can be modeled as a dual-port network [19-20], as shown in Fig. 7. In Fig. 7a, C_{p1} and C_{s1} are the internal stray capacitances of the primary and secondary windings of CT; L_{p1} and L_{s1} are the leakage inductances of the primary and secondary windings of CT; R_{p1} and R_{s1} are the resistances of the primary and secondary windings; C_{ps} is the winding capacitance between the primary and secondary windings; L_{CT} is the magnetic inductance of the secondary side; R_{in} is the load resistance of CT. L_{p1} and R_{p1} are very small, which can be ignored, C_{p1}, $C_{s1}$and C_{ps} can be replaced by C_{CT} [20], therefore, Fig. 7a can be simply expressed by Fig. 7b.

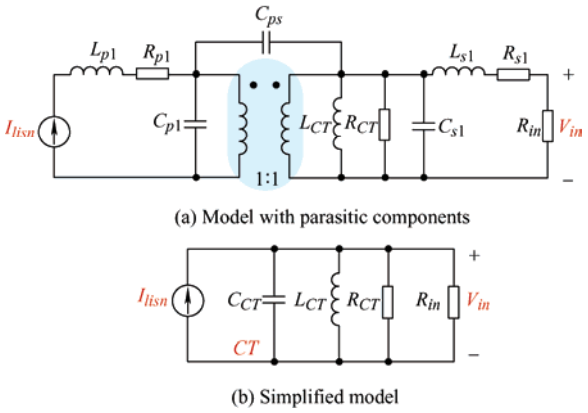

Fig. 7 CM signal sensing model

In view of the noise sensing characteristics of the CT, the turn ratio of the CT is often set as 1∶1. The transimpedance $G_{CT}(s)$ from noise current I_{lisn} to the voltage V_{in} in Fig. 7 can be expressed as Eq. (3)

$$G_{CT}(s)=\frac{V_{in}(s)}{I_{lisn}(s)}=\frac{1}{n}\frac{sL_{CT}R_{CT}R_{in}}{s^2L_{CT}R_{CT}R_{in}C_{CT}+sL_{CT}(R_{CT}+R_{in})+R_{CT}R_{in}} \tag{3}$$

3.2 High-frequency OPAM in DCJ-CSCC AEF

As an active component, the OPAM plays a very important role of obtaining high insertion loss in AEF. However, the frequency bandwidth of an OPAM is limited. Thus, a current-feedback amplifier (CFA) is used in this paper. The CFA has a wider bandwidth than the voltage-feedback amplifier (VFA) [21].

According to the high-frequency equivalent circuit of the OPAM shown in Fig. 8 [15, 21], the closed-loop voltage gain circuit can be expressed as Eq. (4)

$$G_{amp}(s)=\frac{V_{out}}{V_{in}}=\frac{G_{op-amp}}{1+\frac{Z_{op}}{Z_L}+\frac{Z_{op}}{R_1+R_2}+\frac{R_1}{R_1+R_2}\cdot G_{op-amp}} \tag{4}$$

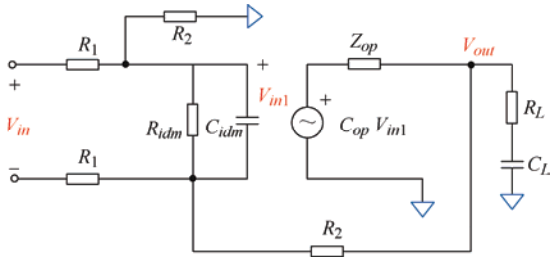

Fig. 8 Circuit model of the amplifier

3.3 Calculation of the insertion losses of AEFs with BJT high-frequency equivalent model

In this part, to obtain the insertion loss expression for describing EMI filtering effect of the proposed AEF, the high-frequency equivalent circuit of the DCJ-CSCC AEF is established, compared with equivalent circuits of FB-CSCC AEF and FF-CSCC AEF.

The proposed DCJ-CSCC AEF is symmetrical for the CM path; therefore, its structure can be equivalent to half for analysis. In the proposed AEF model, the BJT can be replaced by an equivalent circuit model based on the analogue circuit theory, as shown in dotted line box of the Fig. 9.

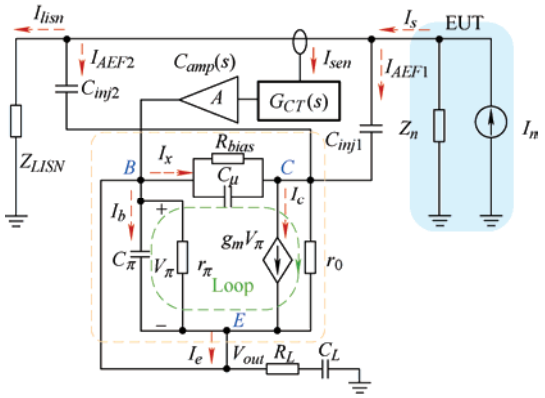

Fig. 9 Equivalent circuit model of the DCJ-CSCC AEF

Fig. 9 shows the high-frequency equivalent circuit of DCJ-CSCC AEF, where $G_{CT}(s)$ and $G_{amp}(s)$ represent the transfer function expressions of the CT and OPAM circuit, respectively. I_n and Z_n represent the equivalent current source and equivalent impedance of the interference source, respectively. The nodes of the base (B), collector (C), and emitter (E) are depicted in Fig. 9. C_μ, R_π, C_π, r_o, and g_m represent the BJT's base-collector capacitance, input resistance, base-emitter capacitance, output resistance and transconductance, respectively [22]. The parameters of the BJT are determined by the BJT bias voltage, and the quiescent point can be selected by adjusting the value of R_{bias}. I_{b1}, I_{c1}, and I_{bias} represent the base current and collector current of the BJT, and the current flowing through R_{bias} and C_μ. I_{lisn1} represents the current flowing into Z_{LISN}, and I_{AEF} represents the injection current of the AEF.

The parameters of the BJTs are given in Tab. 1, where the current gain bandwidth product f_T and output capacitance C_π can be obtained from the datasheet of BJT, and other parameters can be derived from f_T and C_π.

Tab. 1 Circuit parameters of the equivalent circuits

Parameter	Value
Injection capacitor C_{inj1},C_{inj2}/nF	560
Resistor between the collector and base R_{bias}/Ω	1 000
Load capacitor C_L/nF	100
Load resistor R_L/Ω	1
Transconductance g_m/S	0.046
Base-emitter capacitance C_π/nF	34.25
Base-collector capacitance C_μ/nF	35
Base-emitter resistor R_π/kΩ	5.19

According to the current loop in Fig. 9 and Kirchhoff current law (KCL) and Kirchhoff voltage law (KVL), Eqs. (5)-(6) can be obtained.

$$\begin{cases} i_e = g_m V_\pi + i_x \\ i_x = -j\omega C_\mu \cdot V_\pi \\ V_\pi = i_b (r_\pi \,\|\, 1/\, j\omega C_\pi) \end{cases} \tag{5}$$

$$\begin{cases} V_{out} = I_{sen} \cdot G_{CT}(s) \cdot G_{amp}(s) \\ I_c = g_m Z_\pi \cdot I_b \\ I_e = V_{out} / Z_L = I_b + I_c = (1 + g_m Z_\pi) I_b \end{cases} \tag{6}$$

Further, According to the equivalent circuit shown in Fig. 9, Eq. (7) can be obtained.

$$\begin{cases} I_{c1} = I_{AEF1} + I_{AEF2} + I_x \\ Z_{LISN} I_{lisn} = V_{out} + I_b Z_\pi + (-I_x) Z_\mu + I_{AEF2} Z_{inj2} \\ Z_n I_s = V_{out} + I_b Z_\pi + (-I_x) Z_\mu + I_{AEF1} Z_{inj1} \end{cases} \tag{7}$$

Since there are two injection loops in DCJ-CSCC AEF, namely, I_{AEF1} and I_{AEF2}, the transfer function block diagrams of DCJ-CSCC AEF can be obtained by using the superposition principle, as shown in Fig. 10.

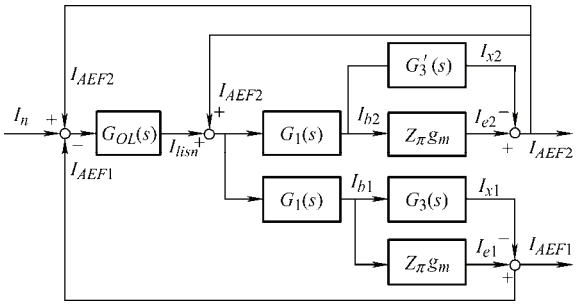

Fig. 10 Block diagram of the proposed DCJ-CSCC AEF

In Fig. 10, $G_{OL}(s)$ represents the voltage division of Z_n and Z_{LISN}. $G_{OL}(s)$, $G_1(s)$, $G_3(s)$ and $G_3'(s)$ are expressed as Eqs. (8)-(11).

$$G_{OL}=\frac{Z_n}{Z_n+Z_{LISN}} \tag{8}$$

$$G_1(s)=\frac{G_{CT}(s)G_{amp}(s)}{Z_L(1+g_mZ_\pi)} \tag{9}$$

$$G_3(s)=\frac{I_{x1}}{I_{b1}}=\frac{g_mZ_\pi Z_{inj1}+G_2(s)Z_\mu}{Z_\mu+Z_{inj1}} \tag{10}$$

$$G_3'(s)=\frac{I_{x2}}{I_{b2}}=\frac{g_mZ_\pi Z_{inj2}+G_2(s)Z_\mu}{Z_\mu+Z_{inj2}-Z_{LISN}} \tag{11}$$

where

$$Z_L=R_L+\frac{1}{sC_L}\quad Z_\pi=R_\pi\|\frac{1}{sC_\pi}\quad Z_\mu=R_{bias}\|\frac{1}{sC_\mu}$$

$$G_2(s)=(Z_\pi+\frac{G_{CT}(s)G_{amp}(s)-Z_{LISN}}{G_1(s)})\cdot\frac{1}{Z_\mu}$$

The insertion loss expression of DCJ-CSCC AEF can be obtained from Fig. 10, as shown in Eq. (12). Note that I'_{lisn} is the current flowing through the LISN without a filter, and I_{lisn} is the current flowing through the LISN with the proposed DCJ-CSCC AEF; therefore, the insertion loss expression Eq. (12) can be obtained through the quotient of I_{lisn} and I'_{lisn}.

$$IL_{dual}(s)=-20\lg\left(\frac{I_{lisn}}{I'_{lisn}}\right)=-20\lg\left(\frac{G_{OL}(s)}{1+G_{OL}(s)\cdot\dfrac{G_1(s)\cdot(g_mZ_\pi-G_3(s))+G_1(s)\cdot(g_mZ_\pi-G_3'(s))}{1-G_1(s)\cdot(g_mZ_\pi-G_3'(s))}}\right) \tag{12}$$

According to Refs. [23-24], the insertion losses of FB-CSCC AEF and FF-CSCC AEF can be expressed by Eqs. (13) and (14), respectively.

$$IL_{FB}(s)=-20\lg\left(\frac{1}{1+G_{OL}(s)\cdot G_1(s)\cdot(g_mZ_\pi-G_3(s))}\right) \tag{13}$$

$$IL_{FF}(s)=-20\lg\left(\frac{1-G_1(s)\cdot(g_mZ_\pi-G_3'(s))}{1+(G_{OL}(s)-1)\cdot G_1(s)\cdot(g_mZ_\pi-G_3'(s))}\right) \tag{14}$$

Based on the deduction of insertion loss, the insertion losses frequency response diagram of three different structures, namely, FB-CSCC AEF, FF-CSCC AEF and DCJ-CSCC AEF, can be obtained, as shown in Fig. 11. The theoretical calculation results show that the DCJ-CSCC AEF has a bigger insertion loss, which means it can suppress the CM EMI much better.

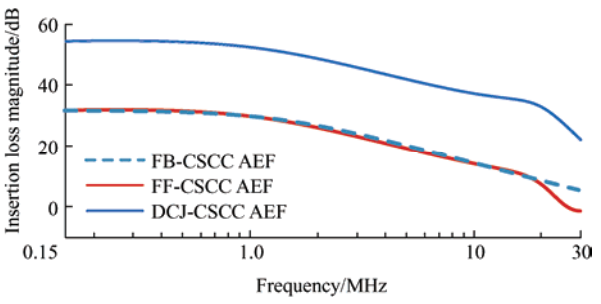

Fig. 11 Insertion loss calculation results

4 Experimental verification and comparison

4.1 Simulation verification of AEFs in a boost converter

To verify the filtering effect of the proposed AEF, DCJ-CSCC AEF was installed in the boost converter, and its overall topology is shown in Fig. 12.

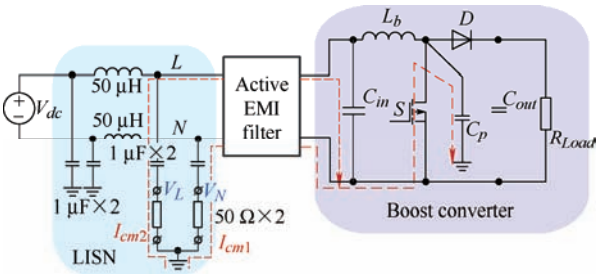

Fig. 12 Illustration of the boost converter with AEF

The main circuit parameters of the boost converter are shown in Tab. 2.

Tab. 2 Operation parameters of boost converter

Parameter	Value
Switching frequency f_s/kHz	100
Input voltage V_{in}/V	24
Input current I_{in}/A	0.5
Output voltage V_{out}/V	78
Input capacitor C_{in}/μF	22
Inductor L_1/μH	300
Load resistance R_{Load}/Ω	44
Output capacitor C_{out}/μF	100

The main circuit parameters of the proposed DCJ-CSCC AEF are shown in Tab. 3.

Tab. 3 Main parameters of the proposed AEF

Component	Parameter	Value
Current transformer	Turning ratios of CT n	1∶1
	Core relative permeability μ	7 912
	Magnetic inductance L_{CT}/μH	157.6
	Stray capacitance C_{CT}/pF	22
	Stray resistor R_{CT}/kΩ	1.56
	Excitation inductance L_m/μH	9.242
	Resistor R_{in}/Ω	1
Operational amplifier	Unit gain bandwidth product *GBP*/MHz	120
	Slew rate *SR*/(V/μs)	7 000
	Supply voltage *Vcc*/V	±15
Push-pull amplifier	DC current gain h_{FE}	240
	Current gain bandwidth product f_T/MHz	100
Injection circuit	Voltage divider R_1, R_2/Ω	1 000
	Load resistance R_L/Ω	0.5
	Load capacitance C_L/nF	200
	Injection capacitance C_{inj}/nF	100

The boost converter with AEFs are analyzed and simulated in ANSYS. According to the measurement circuit in Fig. 12, the CM voltage of boost converter can be obtained as Eq. (15)

$$V_{CM} = (V_L + V_N)/2 \tag{15}$$

The time-domain waveforms of the common mode voltage of boost converter under different AEFs are shown in Fig. 13, and its frequency-domain spectrum is shown in Fig. 14.

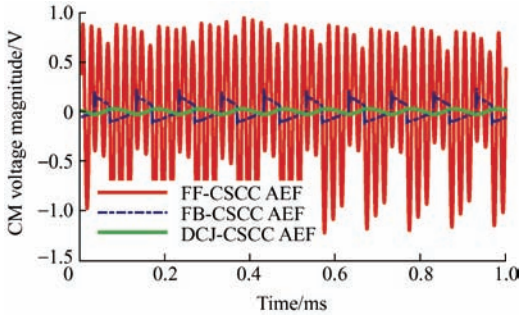

Fig. 13 Simulation results of the CM waveform of boost converter with and without AEFs

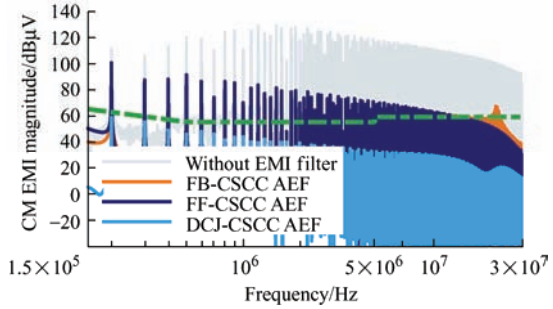

Fig. 14 Simulation results of the CM EMI spectrum of the boost converter with and without AEFs

According to Fig. 14, it can be seen that DCJ-CSCC AEF has better CM EMI suppression effect, which is consistent with theoretical analysis, and only with DCJ-CSCC AEF, the EMI magnitude of the boost converter can satisfy the EMC standard.

In order to further verify the effectiveness and correctness of the proposed AEF, the simulation results and theoretical calculation results are compared. The insertion losses with different AEFs in Fig. 11 can be proved by the difference between the EMI magnitude envelopes of the boost converter under using no AEF and using different AEFs in Fig. 14, the comparison results are shown in Fig. 15, which is almost the same with the calculated insertion losses in Fig. 11.

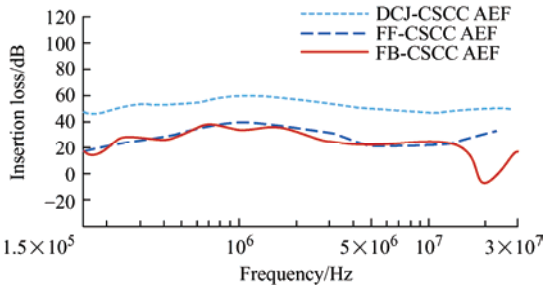

Fig. 15 Insertion loss simulation results

Thus, the CM EMI filtering effect of the DCJ-CSCC AEF can be proved and it really much better than any one of FF-CSCC and FB-CSCC AEFs, its CM EMI filtering effect is comparable to that of a two-stage AEF.

4.2 Implementation of the DCJ-CSCC AEF in boost converter

The AEF platform shown in Fig. 16 was built. The filter volume was 50 mm×60 mm×20 mm, which was roughly the same as the AEF volume of independent FF/FB-CSCC [25]. The actual test platform is shown in Fig. 17.

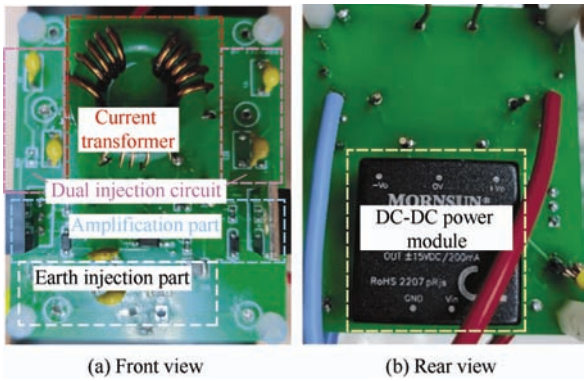

Fig. 16 Proposed AEF platform

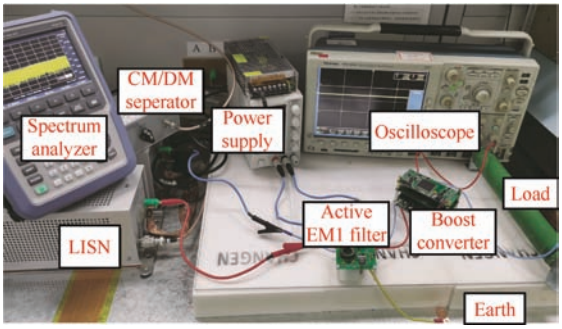

Fig. 17 The test platform of boost converter

Firstly, the injection current of the DCJ-CSCC AEF was tested. Fig. 18 shows the CM voltage waveform of the boost converter before and after installing the DCJ-CSCC AEF. Fig. 18 shows that the peak-to-peak value of the CM voltage exhibited significant attenuation after adding the DCJ-CSCC AEF. In other words, the compensation current injected into the main circuit through the dual injection loop compensated the noise current inversely. The CM current was compensated to a certain extent.

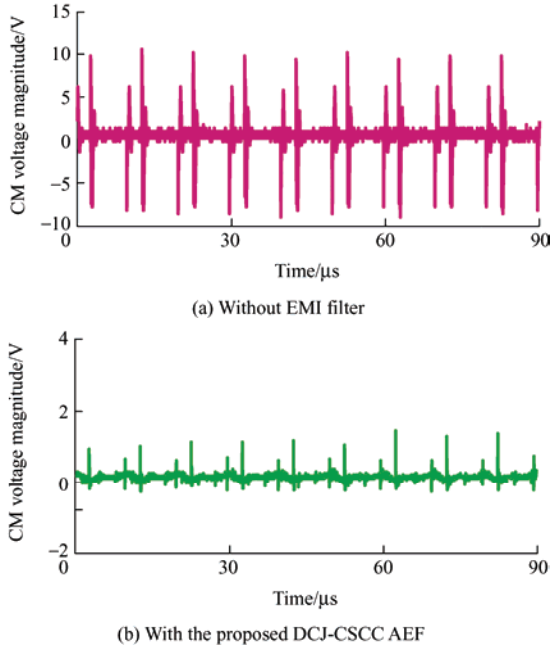

Fig. 18 CM voltage waveform of boost converter

The CM voltage obtained with the proposed DCJ-CSCC AEF was sampled using a spectrum analyzer and then compared with the original noise without the filter. The specific filtering effect of the AEF in the frequency domain is shown in Fig. 19. In particular, the insertion losses at 1.2 MHz and 11 MHz provided by the proposed AEF can achieve 46 dBμV and 35 dBμV, respectively.

Secondly, to prove that DCJ-CSCC AEF has better EMI filtering effect than FF-CSCC or FB-CSCC AEF, we also tested the EMI spectrum of the boost converter under FF-CSCC AEF and FB-CSCC AEF. The same circuit parameters are used in FF-CSCC and FB-CSCC AEFs, but with only one injection loop in the CM EMI tested, and the obtained CM voltage waveforms are shown in Fig. 20.

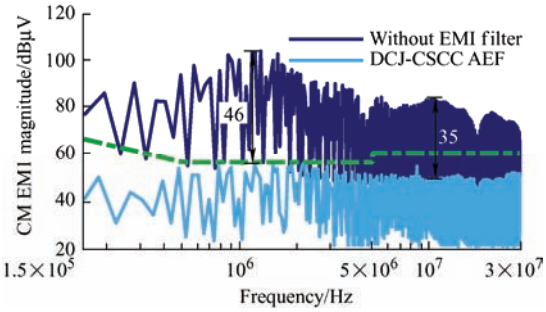

Fig. 19 CM EMI spectrum of boost converter with and without the proposed DCJ-CSCC AEF

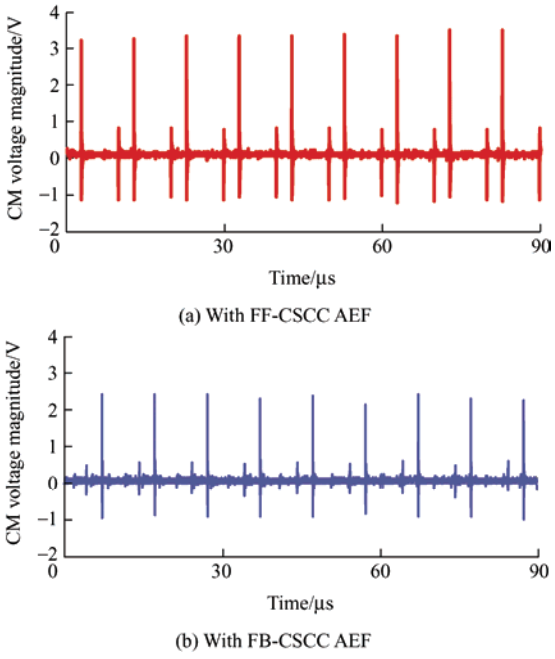

Fig. 20 CM voltage waveform of boost converter

The CM EMI filtering effects of the proposed DCJ-CSCC AEF, FB-CSCC, and FF-CSCC AEFs are compared, and the results are shown in Figs. 21-22.

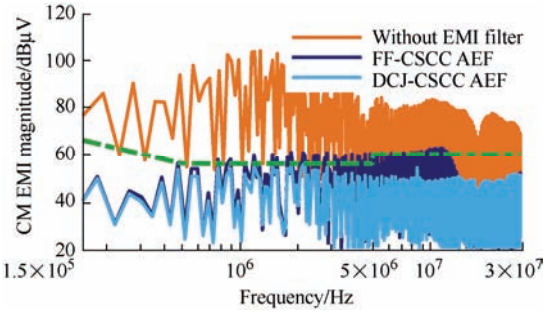

Fig. 21 CM EMI spectrum of the boost converter with the proposed DCJ-CSCC and FF-CSCC AEFs

The experimental results also show that the proposed DCJ-CSCC AEF had a better filtering effect.

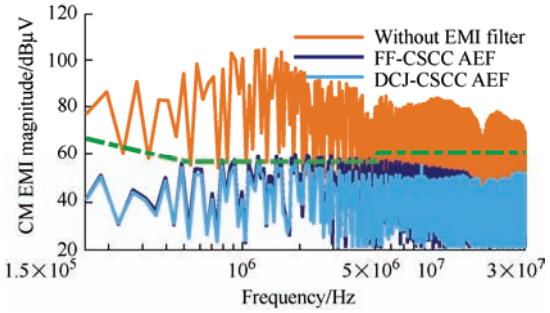

Fig. 22 CM EMI spectrum of boost converter with the proposed DCJ-CSCC and FB-CSCC AEFs

4.3 Experimental results analysis

Based on Fig. 22, it can be observed that the EMI filtering effect of DCJ-CSCC AEF has a certain gap compared with the high insertion loss in the simulation and theoretical calculation. The reason is that the provided instantaneous power from the power supply module of the proposed AEF was not high enough in the actual experiment, which reduce the EMI filtering effect a lot. Since, in simulation all power supply modules are ideal voltage sources, it can provide any current required without limit. However, in the experiment, the maximum output current and output power of the power supply module are only 200 mA and 6 W.

To further prove this opinion above, we set the power limit of the power supply in PSpice simulation, and the EMI filtering effect is shown in Fig. 23 with the power of the power supply is set to 6 W.

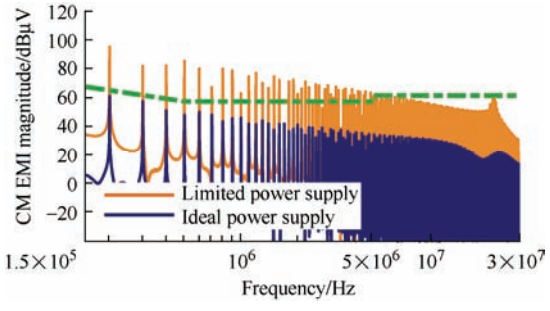

Fig. 23 Simulation results of the CM EMI spectrum with the DCJ-CSCC AEF and different power supplies

According to Fig. 23, it can be concluded that the EMI filtering effect of DCJ-CSCC AEF decreases significantly when the power supply was limited, which can explain the difference between the simulation results and experimental results in this paper.

In addition, considering the limited power of power supply modules, the simulation results of the EMI filtering effects with different AEFs are also given, as shown in Fig. 24. According to Fig. 24, the DCJ-CSCC AEF still demonstrates the best EMI filtering effect among all the AEFs, but effect was smaller than the simulation results in Fig. 14, since the ideal power supply is used in the simulation of Fig. 14, but the results in Fig. 24 are more consistent with the experimental results.

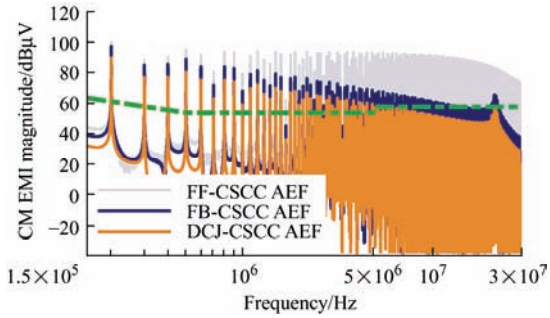

Fig. 24 Simulation results of the CM EMI spectrum of the boost converter with a limited power supply

If we want to improve the EMI filtering effect of the proposed AEF in practice, a power supply module with higher power level can be used. But it should be noticed that there is a balance between the EMI filtering effect and the cost, the volume of the proposed AEF.

5 Conclusions

In this paper, a new DCJ-CSCC AEF is proposed, whose EMI filtering effect are analyzed theoretically and further verified by simulation and experiment based on a boost converter. The proposed DCJ-CSCC AEF has the advantages of compactness and high insertion loss compared with existing single-injection CSCC AEFs. The following conclusions were drawn.

(1) Compared with the existing FF-CSCC AEF and FB-CSCC AEF, in the proposed DCJ-CSCC AEF, only two capacitors are added, and it does not need large-volume CM inductive choke, which makes it easier to achieve higher power density of DC-DC converters.

(2) With the similar volume of AEFs, in the

frequency band of 150 kHz-30 MHz, the proposed DCJ-CSCC AEF exhibits a good EMI filtering effect, and the magnitude of the insertion loss is between 21-46 dBμV, which ensures that the boost converter satisfies the EMC standard, whereas the EMI spectrum of the same boost converter with the FF-CSCC AEF or FB-CSCC AEF exceeds the EMC standard. In particular, the insertion losses at 1.2 MHz and 11 MHz provided by the proposed DCJ-CSCC AEF can achieve 46 dBμV and 35 dBμV, respectively.

(3) The proposed DCJ-CSCC AEF has good universality; it is suitable for all types of DC-DC converters, particularly those with high power densities.

References

[1] J Meng, W Ma. Power converter EMI analysis including IGBT nonlinear switching transient model. *IEEE Transactions on Industrial Electronics*, 2006, 53(5): 1577-1583.

[2] V Serrao, A Lidozzi, L Solero, et al. EMI characterization and communication aspects for power electronics in hybrid vehicles. *2007 European Conference on Power Electronics and Applications*, Sept. 2-5, 2007, Aalborg, Denmark. Piscataway: IEEE, 2007: 1-10.

[3] C Marlier, A Videt, N Idir, et al. Hybrid time-frequency EMI noise sources modeling method. *2013 15th European Conference on Power Electronics and Applications (EPE)*, Sept. 2-6, 2013, Lille, France. Piscataway: IEEE, 2013: 1-9.

[4] D Boroyevich, Z Chen, F Luo, et al. High-density system integration for medium power applications. *2010 6th International Conference on Integrated Power Electronics Systems*, March 16-18, 2010, Nuremberg, Germany. Piscataway: IEEE, 2010: 1-10.

[5] CISPR22. Standard: Information technology equipment Radio disturbance characteristics Limits and methods of measurement. CISPR22: EN55022, 2006.

[6] Y C Son, S K Sul. A new active common-mode EMI filter for PWM inverter. *IEEE Transactions on Power Electronics*, 2003, 18(6): 1309-1314.

[7] V Serrao, A Lidozzi, L Solero, et al. Common and differential mode EMI filters for power electronics. *2008 International Symposium on Power Electronics, Electrical Drives, Automation and Motion*, June 11-13, 2008, Ischia, Italy. Piscataway: IEEE, 2008: 918-923.

[8] C Cuellar, N Idir. Reduction of the parasitic couplings in the EMI filters to improve the high frequency insertion loss. *IECON 2018 - 44th Annual Conference of the IEEE Industrial Electronics Society*, Oct. 21-23, 2018, Washington, DC, USA. Piscataway: IEEE, 2018: 5766-5771.

[9] Y Son, S K Sul. Generalization of active filters for EMI reduction and harmonics compensation. *IEEE Transactions on Industry Applications*, 2006, 42(2): 545-551.

[10] H Hsieh, P Lin, G Hsieh. Design and implementation of the digitally-controlled active EMI filter (DSP-AEF) for noise reduction applications. *2015 IEEE 2nd International Future Energy Electronics Conference (IFEEC)*, Nov. 1-4 2015, Taipei, Taiwan, China. Piscataway: IEEE, 2015: 1-4.

[11] J Ji, W Chen, X Yang. Design and precise modeling of a novel digital active EMI filter. *2016 IEEE Applied Power Electronics Conference and Exposition (APEC)*, March 20-24, 2016, Long Beach, CA, USA. Piscataway: IEEE, 2016: 3115-3120.

[12] B Narayanasamy, F Luo. A survey of active EMI filters for conducted EMI noise reduction in power electronic converters. *IEEE Transactions on Electromagnetic Compatibility*, 2019, 61(6): 2040-2049.

[13] R Goswami, S Wang, Y Zhang. Modeling, analysis and design of differential mode active EMI filters with feedforward and feedback configurations for AC-DC converters. *2016 IEEE Energy Conversion Congress and Exposition (ECCE)*, Sept. 18-22, 2016, Milwaukee, WI, USA. Piscataway: IEEE, 2016: 1-8.

[14] B Narayanasamy, F Luo, Y Chu. High density EMI mitigation solution using active approaches. *2017 IEEE International Symposium on Electromagnetic Compatibility & Signal/Power Integrity (EMCSI)*. Aug. 7-11, 2017, Washington, DC, USA. Piscataway: IEEE, 2017: 813-818.

[15] Y Chu, S Wang, Q Wang. Modeling and stability analysis of active/hybrid common-mode EMI filters for DC/DC power converters. *IEEE Transactions on Power Electronics*, 2016, 31(9): 6254-6263.

[16] L Dai, W Chen, X Yang, et al. A multi-function common mode choke based on active CM EMI Filters for AC/DC power converters. *IEEE Access*, 2019, 7(3): 43534-43546.

[17] H Li, C Zhang, Y Ding, et al. Optimization of high frequency noise suppression effect of active EMI filter

based on chaotic spread spectrum PWM method. *IEEE Transactions on Power Electronics*, 2022, 42(13): 4642-4652.

[18] Y Zhou, W Chen, X Yang. Investigation of cascade connection method to improve the insertion loss of DM active EMI filters. *IEEE Journal of Emerging and Selected Topics in Power Electronics*, 2022, 10(1): 1084-1094.

[19] A Vedde, M Neuburger, C Cheshire, et al. Optimization of a passive common mode EMI filter by adding an active feedback loop. *2021 IEEE Southern Power Electronics Conference (SPEC)*, December 6-9, 2021, Kigali, Rwanda. Piscataway: IEEE, 2021: 1-6.

[20] R Goswami, S Wang, Y Chu. Design of an active differential mode current filter for a boost power factor correction AC-DC converter. *2015 IEEE Energy Conversion Congress and Exposition (ECCE)*, 20-24 September, 2015, Montreal, QC, Canada. Piscataway: IEEE, 2015: 4375-4382.

[21] E Sanchez-Sinencio, M Majewski. A nonlinear macromodel of operational amplifiers in the frequency domain. *IEEE Transactions on Circuits and Systems*, 1979, 26(6): 395-402.

[22] S P Voinigescu, M C Maliepaard, J L Showell, et al. A scalable high-frequency noise model for bipolar transistors with application to optimal transistor sizing for low-noise amplifier design. *IEEE Journal of Solid-State Circuits*, 1997, 32(9): 1430-1439.

[23] D Shin, S Jeong, J Kim. Quantified design guidelines of a compact transformerless active EMI filter for performance, stability, and high voltage immunity. *IEEE Transactions on Power Electronics*, 2018, 33(8): 6723-6737.

[24] D Shin, S Kim, G Jeong, et al. Analysis and design guide of active EMI filter in a compact package for reduction of common-mode conducted emissions. *IEEE Transactions on Electromagnetic Compatibility*, 2015, 57(4): 660-671.

[25] H Li, Y Ding, C Zhang, et al. A compact EMI filter design by reducing the common-mode inductance with chaotic PWM technique. *IEEE Transactions on Power Electronics*, 2021, 37(1): 473-484.

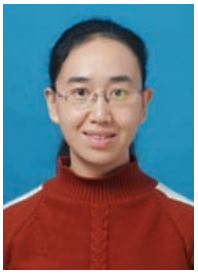

Hong Li received the B.Sc. degree in Electrical Engineering from Taiyuan University of Technology, Taiyuan, China, in 2002, M.Sc. degree in Electrical Engineering from South China University of Technology, Guangzhou, China, in 2005, and Ph.D. degree in Electrical Engineering from Fern Universität in Hagen, Germany, in 2009.

She is currently a Full Professor with the School of Electrical Engineering, Beijing Jiaotong University, Beijing, China. She has published 1 book, 68 journal papers, and 61 conference papers. She has also authorized 30 patents. Her research interests include nonlinear modeling, analysis and its applications, EMI suppressing methods for power electronic systems, and wide bandgap power devices and applications.

Dr. Li is an Associate Editor of the IEEE Transactions on Industrial Electronics, an Associate Editor of the IEEE Open Journal of Industrial Electronics Society, an Associate Editor of the Chinese Journal of Electrical Engineering, and the Vice Chairman of Electromagnetic Compatibility Specialized Committee in China Power Supply Society.

Siyi Wang was born in Zhejiang Province, China, in 1998. He received the B.S. degree in Electrical Engineering from Zhejiang Sci-Tech University, Hangzhou, China, in 2021. He is currently working toward the M.S. degree in Electrical Engineering at the School of Electrical Engineering, Beijing Jiaotong University, Beijing, China. His research interest is the design of EMI filters in power electronics.

Chongmo Zhang was born in Liaoning Province, China, in 1998. She received the B.S. degree in Electrical Engineering from Beijing Jiaotong University, Beijing, China, in 2020. She is currently working toward the M.S. degree in Electrical Engineering at the School of Electrical Engineering, Beijing Jiaotong University, Beijing, China. Her current research interests are electromagnetic compatibility and EMI filters in power electronics.

Bo Zhang (M'03-SM'15) was born in Shanghai, China, in 1962. He received the B.Sc. degree in Electrical Engineering from Zhejiang University, Hangzhou, China, in 1982, M.Sc. degree in Power Electronics from Southwest Jiaotong University, Chengdu, China, in 1988, and Ph.D. degree in Power Electronics from Nanjing University of Aeronautics and Astronautics, Nanjing, China, in 1994.

He is currently a Professor of the School of Electric Power Engineering, South China University of Technology, Guangzhou, China. He has authored or coauthored more than 380 papers and 80 patents. His research interests include nonlinear analysis and control of power supplies and AC drives.